Communications in Physics, Vol. 31, No. 3 (2021), pp. 289-300
DOI:10.15625/0868-3166/15768

MAGNETIC DOMAIN WALLS MOVING IN CURVED PERMALLOY NANOWIRES UNDER CONTINUOUS AND PULSED FIELDS

DUC-QUANG HOANG[1,†], XUAN-HUU CAO[2,3], HOAI-THUONG NGUYEN[4] AND VINH-AI DAO[3,5]

[1]*Applied Computational Civil and Structural Engineering Research Group, Faculty of Civil Engineering, Ton Duc Thang University, Ho Chi Minh City 700 000, Vietnam*

[2]*Institute of Research and Development, Duy Tan University, Da Nang 550 000, Vietnam*

[3]*Faculty of Electrical-Electronic Engineering, Duy Tan University, Da Nang 550000, Vietnam*

[4]*Faculty of Electrical Engineering Technology, Industrial University of Ho Chi Minh City, Ho Chi Minh City 700 000, Vietnam*

[5]*Future Materials & Devices Laboratory, Institute of Fundamental and Applied Sciences, Duy Tan University, Ho Chi Minh City 700 000, Vietnam*

E-mail: [†]hoangducquang@tdtu.edu.vn

Received 19 December 2020

Accepted for publication 19 January 2021

Published 18 April 2021

Abstract. *Magnetic domain walls created and propagated in curved permalloy nanowires under continuous and pulsed fields in a Lorentz microscope. Using such nanowires aims to create a single or multiple magnetic domain walls in typical areas of those structures, an external magnetic field then applies along the long axis of these nanowires. Following that the created domain walls are propagated from one end to the other end of each wire by increasing the continuous/pulsed field strength. At each increased field value, a Fresnel image is recorded. The obtained results show that the characteristics of those created and propagated domain walls are dependent on various parameters, i.e. connecting structures, wall types and chiralities. Corners between the straight and linking sections of those curved nanowires also play a crucial role along with the local defects created in these wire-edges and surfaces where a point-defect is considered as a potential well that could pin/distort those created/propagated domain walls. By the aid of these observations, the dynamic properties of domain walls with the creating and propagating processes in those curved nanowires are exposed. These outcomes are vital to design novel domain wall trap structures supporting reproducible domain wall motions. That are of interest in providing a better understanding of multiple bits moving in the future 3D racetrack memory, logic gates, shift register and other spintronic/computing devices.*

Keywords: domain walls; spintronics; Lorentz microscope; nanostructures; alloy.

Classification numbers: 75.70.Kw; 85.75.-d; 07.78.+s; 61.46.-w; 75.50.Bb.

I. INTRODUCTION

The soft ferromagnetic permalloy (Py) material - $Ni_{80}Fe_{20}$ has many applications in the new generation magnetic recording technology [1–3]. The propagation of boundaries between two quasi-homogeneous magnetic order regions characterized by magnetization vectors ($\mathbf{M_i}$), the so-called magnetic domain wall (DW), is of interest. The properties of such DWs have been attracting much attention recently [4–12]. This material has been extensively studied on large samples and having many undiscovered properties in small ones. The geometry and propagation characteristics of DWs in nanowires are particularly interested in many outstanding research groups. The fundamental parameters relating to the propagation of DWs in nanostructures with different shapes/sizes are strongly concerned. In writing/reading information devices, a DW is considered as an entity – the boundary between the 'bits' of information, as depicted in Fig. 1. Therein, DWs stored in traditional (2D) and future (3D) magnetic devices and NOT logic gates [1, 2] are seen. The operation of the 2D devices is attributed to be related to the surface properties of reading/writing parts of these devices. An advantage of the novel 3D recording/reading devices, proposed by Stuart S. P. Parkin and his colleagues [1] is that information is stored in 3D columns counting from the surface of 2D traditional devices. The propagation of DWs in such 3D structures is possibly realized by spin-polarized currents. With this method, the movement of DWs is faster than that moved in the traditional one. If such nanostructures are used, the writing/reading information in these 3D devices is processed faster than in traditional ones. Therefore, studying the intrinsic properties or propagation of DWs under the influence of external factors is essential using either continuous/ pulsed current/ magnetic field.

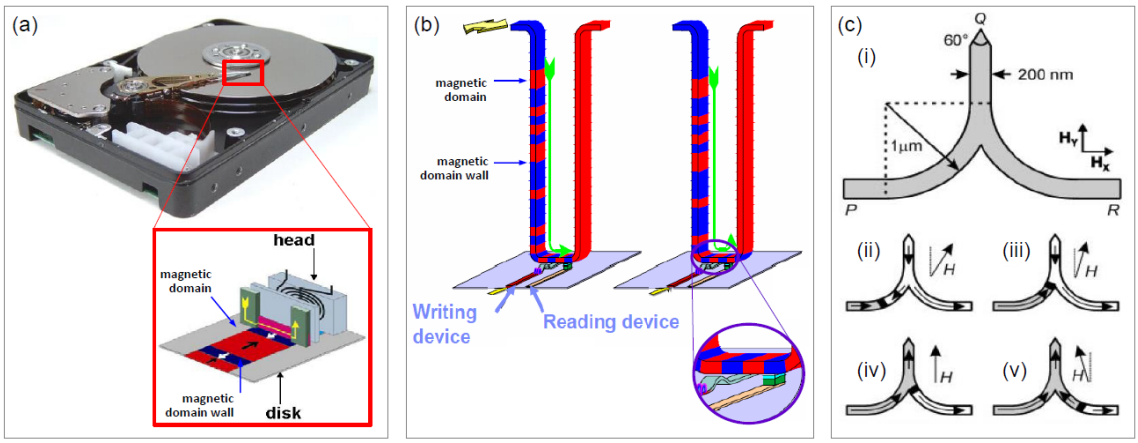

Fig. 1. Simplified diagrams of 2D, 3D and NOT logic gate devices: (a) a 'bit' information is considered as an entity, similar to a DW, is a bound of two neighbouring areas with different magnetic vectors (M_i) moving in a traditional 2D magnetic reading/writing device; (b) A novel 3D magnetic simulated structure proposed by Stuart S. P. Parkin and his colleagues [1] consisting of reading/ writing parts, this aims to increase the reading/writing capacity of the novel generation recording devices; (c) A diagram describing the operation principle of the 2D NOT logic gate [2], the M_i in the device are controlled by the rotation of an external magnetic field, $H_{x,y}$.

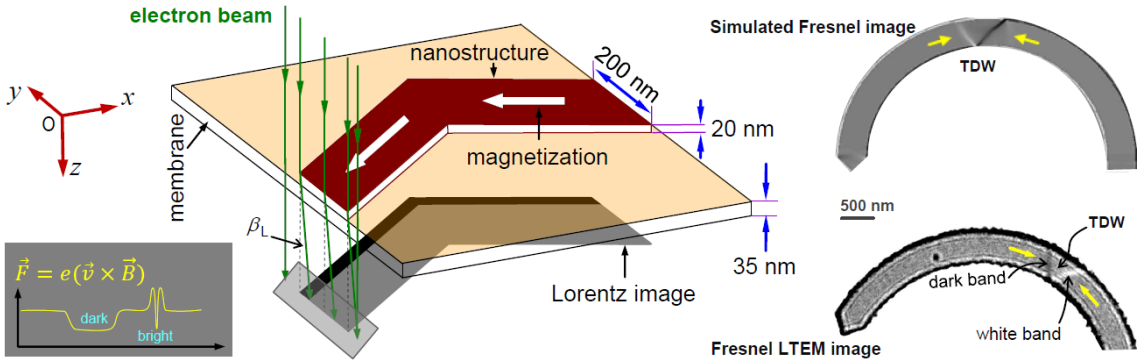

Fig. 2. A simplified diagram of the Fresnel mode in our Lorentz TEM at which an electron beam is deflected when interacting with the intrinsic magnetic moment of a 2D nanowire, satisfying the classical formula of Lorentz force, **F** = -e(**v**×**B**). The e-intensity profile recorded at a plane below the sample is attached in the left-corner. Moreover, the simulated and experimental Fresnel images of 500 nm-width curved nanowire are also shown in the right panel where the bright/dark bands are visible. Therein, a transverse DW (TDW) can also be distinguished from the images based on their magnetic contrast produced by a correlation of the electron intensity levels as compared to the grey background with brighter/darker edges on either side. The bright/dark band is generated from the convergence/divergence of the electron beam, detailed in the text.

The creation of DWs is highly dependent on the shape and size of nanowires (NWs). Therein, the shape anisotropy significantly induces the creation and movement of DWs if the considering structure is fabricated in the nanoscale [1–6]. This is one of the research topics that attracted much interest in materials science, nanotechnology and/or nanomagnetism for more than a decade. Hence, understanding the properties of Py at the nanoscale size with a rapid DW motion is essential [1, 4–8]. Many characterization techniques are used in research, for examples, Magneto Optical Kerr Effect (MOKE), X-ray Magnetic Circular Dichroism (XMCD), Scanning Electron Microscopy with Polarization Analysis (SEMPA) [2, 4–6]. These techniques are used for the direct observation of the magnetic properties of Py structures where the structural and geometric properties of DWs and their dynamics are thus characterized. A well-known magnetic imaging technique, the Lorentz transmission electron microscope (LTEM) [9] is also used. Using this technique allows us to obtain the configuration of DWs in high resolution. The principle and mechanism of Fresnel images are shown in Fig. 2.

II. STRUCTURAL DESIGNS

Various Py nanostructures in shape were designed, simulated and patterned, aiming at optimizing fundamental parameters for those structures. The designed structures were simulated using the Object Oriented Micro-Magnetic Framework (OOMMF) package [10]. The patterned structures were characterized with the Fresnel mode of a Lorentz microscope [11, 12]. Those studying structures are come from an initial nanotrap where a single DW can be created, trapped or moved in such structures – domain wall traps (DWTs) [9]. This was successfully investigated by our colleagues. The movement of the created DW was well driven by an external magnetic field. As shown in Fig. 3, a Fresnel image of the given structure is recited from Ref. [9] where a single DW

created in the middle area of a straight nanowire (NW) with a surface of 200×1000 nm^2 and this NW was connected to diamond pads on either end. The width of those diamonds is about 500 nm. A single DW is able to be created in the NW of this structure if an external magnetic field ($\boldsymbol{H}$) is applied biasing a small angle ($\pm\alpha$) in respect of the vertical direction, denoted as red/blue arrows in Fig. 3(a, b). When an external field is applied, the spins/magnetizations of those two diamond pads will be pushed/pulled from both sides to create a DW with head-to-head (H2H) or tail-to-tail (T2T) DW configuration [9], Fig. 3(c).

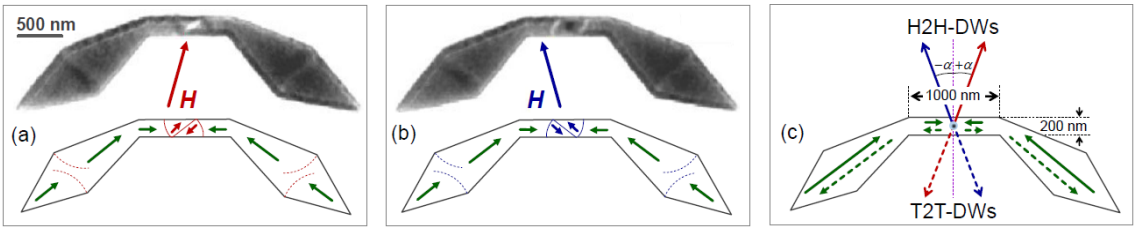

Fig. 3. (a, b) An external field (H) w as oriented at a certain angle ($\pm\alpha$) to the hard-axis of the DWT to change its magnetic configuration. Therein, H2H-VDWs formed in the middle area of the structure are dependent on the α-orientation. (c) A simple schematic of α-aligned fields applied to the structure to obtain H2H-DWs (solid arrows) and T2T-DWs (dashed arrows).

However, how single DW is able to propagate between such NWs through a certain shaped-structure that is one of our research aims. Herein, we extended the initial DWT by adding two other ones at the right-end of the said DWT. The resulting structure consists of five NWs and six diamond pads, as seen in Fig. 4(a). Moreover, the left-end diamond pad was removed and replaced by a square injection one, Fig. 4(b). These structures were patterned using an electron-beam lithography (EBL) method on the Vistec VB6 UHR EWF technique with the FEG voltage is in the range of 50-100 keV [13]. Using this technique, a spartial resolution of 3 nm can be achieved, this allows us to have an acceptable roughness for patterned structures. All fabrication processes were realized at the Glasgow James Watt nanofabrication center, realized by Dr. Kerry J. O'Shea. In principle, the desired DWTs are designed to retain the evaporated Py material on a Si_3N_4 membrane, the continous Py thin film outside the designed DWTs is erased. In fact, effects of re-deposition can be created at the edges of patterned structures during the fabrication. With this EBL technique, the effect of redepositon is less as compared to the focussed ion beam (FIB) patterning method [14].

Many wall types can be created in the same 2D Py NWs, i.e. vortex and transverse walls (VDW, TDW) [3]. There are two VDW types, i.e. clockwise and counter-clockwise VDWs (CW- and CCW-VDWs). The TDW has symmetric and asymmetric configurations (STDW and ATDW) [3, 11]. For each wall type, two possibilities of magnetization vectors ($\boldsymbol{M_{1,2}}$) in either side of a DW are generally considered as head-to-head (H2H) and tail-to-tail (T2T) states, the so-called H2H and T2T-DWs [3,9]. Typical DW types often appear in NWs are depicted in Fig. 5. If the thichkness of NWs is varied in the range of 10-20 nm, the possibility of TDWs is highly obtained. Moreover, those wall types can coexist in the same structure where an important factor highly induces the coexistence of those DWs is the edge roughness as directly affected the speed of DWs in the designed and fabricated structures. The operation of future recording devices is highly

dependent on the creation, propagation and transformation processes of those DWs [15]. Such diversities are therefore opened up new research directions in the spintronic discipline [1, 2, 7].

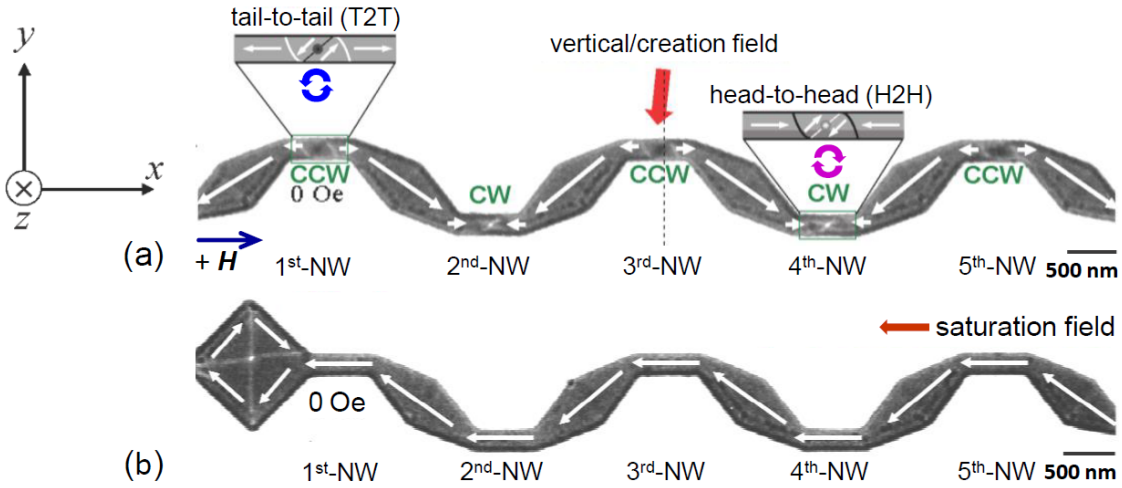

Fig. 4. (a) A Fresnel image of the DWT without a square injection pad consists of five nanowires (NWs) and six diamond pads where tail-to-tail (T2T) and head-to-head (H2H) VDWs alternatively created at the middle areas of those NWs from the first to fifth NW with the creation field applied vertical to the easy axis of the structure. (b) Anothe Fresnel image of the DWT with a square injection pad consists of five NWs and five diamond pads. Herein, the DWT saturated by a saturation field of 5.5 kOe applied along the easy axis of the structure in the right-to-left direction. The magnetization state in the square injection pad shows as a flux-closure with head-to-tail wall structures, depicted as four white arrows. A single DW can create at the left-end of the 1st-NW if an external field applies along the left-to-right direction, indicated as a blue arrow. Propagation of those DWs under the horizontal field is then studied. Results of which are discussed in the text.

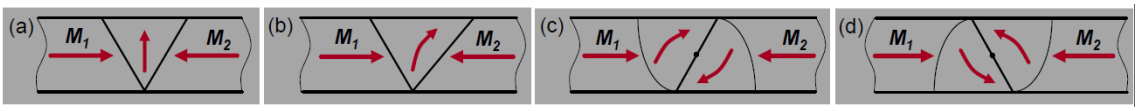

Fig. 5. Three types of H2H-DWs: (a) symmetric TDW (STDW); (b) Asymmetric TDW (ATDW); (c, d) clockwise and counter-clockwise VDW (CW and CCW-VDWs). Here, if the STDW or ATDW is divided into two halves by a virtual line passing through the TDW vertex, then the correlation of those two halves shows whether it is symmetric or asymmetric: if those two halves are equal, a STDW is obversed, whereas if those two halves are unequal, an ATDW is obtained [10].

III. EXPERIMENT

Those 20 nm-thick DWTs were fabricated following in a couple steps: (*i*) a continuous Py film evaporated on a transparent Si_3N_4 TEM membrane using an evaporator with the evaporation rate of 0.3 Å/s. Using such membrane is useful for LTEM characterization at which the Si_3N_4 substrate is an amorphous film with a thickness of 35 nm supported by the 500 μm-thick Si frame

with a window of 100×100 μm^2 [12], purchased from TED PELLA, INC. [16]. A schematic of the 20 nm-thick Py film deposited on the Si_3N_4 membrane is depicted in Fig. 6. Herein, the thickness of evaporating film is monitored by controlling a correlation of the quartz crystal film vibration and material deposited into the quartz film. The correlation of the mechanical vibration and the resonant frequency of the quartz film was monitored as a function of time. As mentioned, using the transparent Si_3N_4 substrate allows a direct observation of the magnetic and structural characteristics of Py films in our LTEM, the Si_3N_4 amorphous material will not affect the contrast of the Lorentz image. (*ii*) The DWTs were then patterned using the EBL method, as described in subsection II.1. Magnetic properties of those structures were measured with the Fresnel mode of Philips CM20 [17] with a defocused distance of 3.6 mm (Δ). To prevent the effects of charging on the Py DWT structures during the EBL fabrication and LTEM characterization processes, a 10 nm-Au-thick was evaporated onto the backside of the Si_3N_4 membrane.

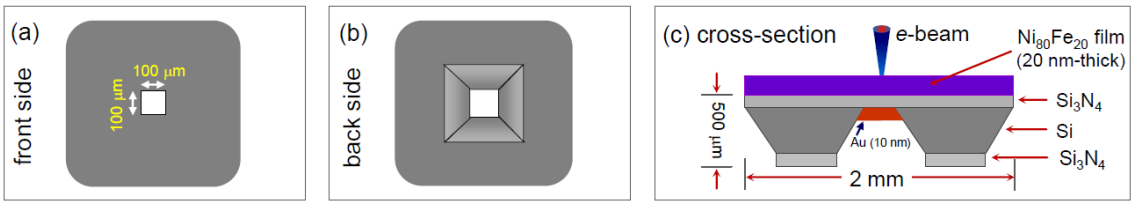

Fig. 6. A Si_3N_4 TEM membrane was used to sputter a Py continuous film on top, the Py film was then patterned by EBL: (a) front and (b) back views of a Si_3N_4 membrane, (c) cross-section of the 20 nm-thick Py film sputtered on the front and 10 nm-thick Au layer deposited on the backside of the Si_3N_4 membrane, the film is illuminated by the e-beam of LTEM from the front.

The magnetic properties of the patterned DWT nanostructures were measured in the modified Philips CM20. The technique was modified for the magnetic imaging purpose [17]. The sample was slipped into a double-tilt TEM holder and the holder was slightly inserted into the LTEM column. The sample was located between two objective lenses of the Philips CM20. This means that the magnetic film can be immersed in a high magnetic field strength of 20 kOe from the said objective lenses applied along the optical axis of the microscope. This large magnetic field can destroy the magnetic state of most soft magnetic samples. The objective lenses were thus switched off and two mini-lenses were replaced to take the role of those objective lenses. Herein, the two-mini lenses play a new function as an imaging lens for the Fresnel and differential phase contrast (DPC) imaging modes [17]. The image principle of the Fresnel mode can be described as, (*i*) the electrons are extracted from the 200 keV FEG source of the LTEM pass through the 20 nm-thick magnetic film; (*ii*) the electron beam is deflected with an angle of β_L satisfying the classical Lorentz force created from the magnetic field around the magnetic nanostructure, as shown in Fig. 2. The magnitude of β_L can be quantified via a relation, $\beta_L = eB_S\lambda t/h$ [17]. e is the elementary charge of -1.602×10^{-19} C, $B_S = \mu_0 M_S$ is the saturation induction, μ_0 is the permeability, M_S is the saturation magnetization, λ is the wavelength of electrons extracted from the 200 keV FEG, $\lambda_{200keV} = 2.51$ pm, t is the sample thickness of 20 nm, h is the Planck constant of 6.626×10^{-34} J s. Besides, $\Delta = 3.6$ mm is used for the Fresnel mode to increase the magnetic contrast of a Fresnel image. This implies that there no magnetic contrast in the in-focused Fresnel image. As shown in Fig. 2, when an e-beam passed through a thin magnetic sample consists of 180°-wall, the e-beam

was deflected with an angle of β_L induced by the Lorentz force. The transmitted electrons were thus separated in two opposite directions. Therefore, the electron intensity profile obtained from the camera plane consists of convergent and divergent bands and they appear as bright and dark areas against the neutral background, as depicted in the left panel of Fig. 2. Moreover, the Fresnel OOMMF simulation and LTEM experimental images for a 500 nm-width curved NW are shown in the right panel of Fig. 2. Herein, the created H2H-TDW is clearly distinguished by white and dark bands crossing the NW width from their vertices.

The patterned structures were mounted to a LTEM rod, this rod is rotable in the left-to-right and up-to-down sides. The rotation increases the angle (θ) of the magnetic sample plane and optical axis of the LTEM at which the magnetic field direction is always vertical to the horizontal plane. As stated, the magnetic sample is magnetized under the magnetic field of the mini-lenses where the strength of the applied magnetic field is adjusted by the dc-current injected from the wires wrapping around those mini-lenses. The magnetic field ($\boldsymbol{H}$) is thus separated into the two components applied perpendicular ($\boldsymbol{H}_{\perp}$) and parallel ($\boldsymbol{H}_{//}$) to the specimen plane and these field components are related to θ. The magnetic field is produced from those lenses perpendicular to the sample plane, no horizontal magnetic field component is applied in the given plane. if the specimen plane is rotated with an angle of $\theta \neq 0^{\circ}$, the parallel magnetic field component ($H_{//}$) is related to the magnetic field (H) of the mini-lenses, $H_{//} = Hsin(\theta)$. The maximum value of $H_{//}$ is reached if $\theta = 90^{\circ}$. The maximum field value of our mini-lenses can be achieved, $H_{\max,//} = 7$ kOe.

The patterned DWT with a square injection was also characterized using the pulsed field method [18], this method integrated in the Lorentz CM20. Herein, various bundles of field pulses are generated with a certain time-period, μs or ns. The dynamic characteristics of created DWs in the studying DWTs may be exposed in the μs/ns-time scale. These pulses were produced by pulsed dc-current from the two parallel-Au wires located below the sample plane, those Au-wires are connected to an agilent function generator [13]. This device can be generated arbitrary waveforms with a particular frequency or amplitude and controlled by a 100A power supply. The stage of those Au-wires is fixed and paralleled to the substrate/sample surface. The maximum pulsed field of 200 Oe could be generated in the sample plane with the duration range of 0.1–5 μs [18]. Using the combination of these continuous and pulsed field methods is useful to understand the domain wall behaviour and responses of the given structures with both static and pulsed fields.

IV. RESULTS AND DISCUSSION

The patterned DWT without a square injection pad, as seen in Fig. 4(a), shows that those DWs nucleated at the centers of the five NWs. Based on the magnetic contrast of the given image, looking from left to right, T2T- and H2H-VDWs were created as CCW- and CW-chiralities, respectively. Therein, an external magnetic field of 5.5 kOe was applied in the direction quasi-perpendicular to the length of the DWT, indicated as a big red-arrow in Fig. 4(a). The spin states of these VDWs show that the external magnetic field was applied biasing with a small angle in respect of the vertical direction. Since those DWs created, the quasi-perpendicular magnetic field was turned off and a Fresnel image of the entire DWT was recorded at its relaxed state. Another external magnetic field was then applied from left-to-right to move those DWs from left-to-right (forward) or vice-versa (reverse). Some asterisks are used to denote the movement of those DWs

along the length of the DWT. As shown in Fig. 7, those DWs did not move simultaneously, as compared to the incremental change of the applied field strength. The results showed that the average magnetic field of 19 Oe needs to move those DWs from the central positions of the NWs to their ends. This observation is consistent with the results obtained from the original DWT in Ref. [9]. The external magnetic field was continuously increated to remove those DWs. As a result, the DWs located in the 2^{nd} to 5^{th}-NWs were early annihilated, whilst the DW located in the 1^{st}-NW was removed latterly. The range of those magnetic field strengths required to remove those DWs is small. If the magnetic field increases with a small step of 0.4 Oe, those DWs are however removed at the same magnetic field. The average value of those fields is of 84 Oe, this field value is enough to remove those DWs from the structure, that is very close to the results obtained earlier [9].

In the reversal process, the procedure used to create DWs was repeated exactly what has been done before to get the same state as the previous one. Another external magnetic field applied from left-to-right and gradually increased to 34 Oe, those created DWs shifted in different directions where T2T-DWs moved from left-to-right whilst H2H-DWs moved in the opposite direction. The asynchronous movement mechanism of those DWs in such structures is not systematically studied yet. Based on the results obtained from the single DW propagation between the two 200 nm-width NWs connected by the modified diamond pads, we found that the propagation of single DWs is not only induced by the external field but also influenced by the magnetizing processes in those diamond pads [15]. Therein, the spins in those diamonds slowly rotate in the direction of an external field, this process is asymmetric due to the symmetries of those pads. Besides, the angle of those NWs and diamond pads is also an important factor. However, we do not discuss the influence of such parameters in the scope of this article in detail. As a result, those DWs shifted to the ends of these NWs in the reversal process with the field value of -24 Oe. The difference between the field strengths in the forward ($+34$ Oe) and reversal (-24 Oe) processes can be induced by the hysteresis properties of magnetizing processes in those highly anisotropic DWT nanostructures. We repeated each process for four times to ensure the data in the accurate and repeatable manners.

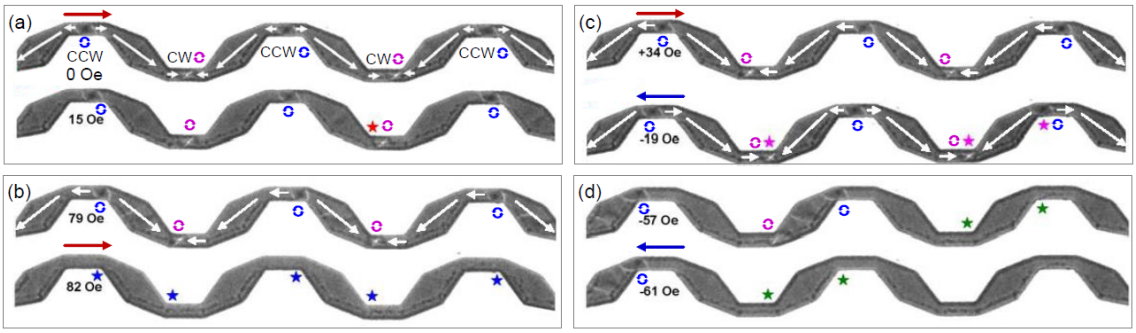

Fig. 7. Fresnel images of the patterned DWT without a square injection pad in different field values that applied on those created DWs: (a) moving, (b) removing, (c) switching, (d) annihilating processes in five NWs. Some asterisks are used to denote the movement of those DWs.

The obtained results clearly show that the propagation behaviour of multiple DWs in the DWT without a square injection pad is asymmetric that might induce by the anisotropic and hysteresis characteristics of the magnetizing process in differing wall types (H2H-DW and T2T-DW)

and spin configurations (CW-VDW and CCW-VDW). To simplify those sophisticated characteristics of multiple DWs occurred at the same time, a square injection geometry was designed and attached to the left-end of the first NW, as shown in Fig. 4(b). This square pad plays a role as a pumper producing a single DW for the remaining part of the DWT. The creation process of a single DW in the said structure is followed in few steps: (*i*) an external magnetic field applies in the right-to-left direction until the structure is saturated, Fig. 4(b); (*ii*) the structure is relaxed when the external field is turned off, and another magnetic field is then applied in the opposite side; (*iii*) the propagation process of a created DW in the said DWT is shown and described in Fig. 8.

The relaxed state of the structure describes the quasi-stable stage where the magnetic configuration of the square injection pad appears as a flux-closure. The spins in the square are oriented clockwise around the core of the said square pad and virtually divided in four quasi-equal parts with four bright fringes (H = 0 Oe). When the magnetic field is increased to H = 66 Oe in the left-to-right direction, the magnetic configuration in the square changes significantly, as seen in Fig. 8(a). Therein, the upper two parts in the pad tend to increase their areas while the areas of the two-lower ones therefore decrease. Particularly, a H2H-DW was created by the white fringe connecting the core of the pad and the upper edge of the first NW. However, the chirality of the created H2H-DW is unknown where the Fresnel image contrast is insufficient to distinguish the spin configuration in the narrow 200 nm-width of the first NW. Therein, the magnetic contrast is fuzzied from the dark and bright fringes at either edge of the first NW. Increasing the external magnetic field up to 93 Oe, Fig. 8(b), the created DW was slightly moved to the middle area of the first NW and its spin configuration was distorted under the pressure of the external field. The magnetic states in those diamond parts were significantly changed, as compared to the states of the DWT under the lower fields. The remaining part of the DWT was strongly magnetized. H = 95 Oe, the DW moved through three diamond pads and four NWs unstopping at any intermediate area, Fig. 8(c). The DW finally stopped at the left end of the fifth NW, denoted as purple stars. The spin configurations inside the square pad largely changed are clearly visualized. This DW was strongly pinned at the given end before ejected out the structure with the field strength of H = 109 Oe, leaving the magnetic state of the DWT is quasi-stable, constrast to the configuration of the structure already showed in Fig. 4(b).

The possibility of conrolling a DW moves to a particular area of the said DWT using a continuous magnetic field did not impove, as discussed in Fig. 8. Hence, the pulsed field method was used to study the influence of pulsed field strengths on the DW propagation of a created DW in the given DWT. The saturation process was done to obtain the initial state of the DWT, as seen in Fig. 4(b). Following that the pulsed magnetic field was applied in the left-to-right direction and gradually increased from 0 Oe to 107 Oe with the increasing field step of 0.4 Oe, Fig. 9. The Fresnel images of the DWT recoreded at $H_{\text{pulsed}} = 0$ Oe and H_{pulsed} = 107 Oe are shown in Fig. 9a$_{\text{I}}$ and Fig. 9a$_{\text{II}}$, respectively. We found that there is no difference between those images, and this might come from the duration of each field pulse is short, t_{pulsed} = 5 μs. When the pulsed field increases to H_{pulsed} = 107.3 Oe (Fig. 9a$_{\text{III}}$), the magnetic configuration in the square pad changes at which the bright fringe connecting the square center and the upper edge of the first NW moved to the lower edge of the first NW. At the same time, the magnetic contrast of the remaining part changes, the white fringe at the DWT upper edge replaced by the dark one. This hints that the magnetic configuration of the DWT was changed. However, we did not obseve any DW moving to any location in the remaining part of the DWT. This means that using the field pulses of 5-μs

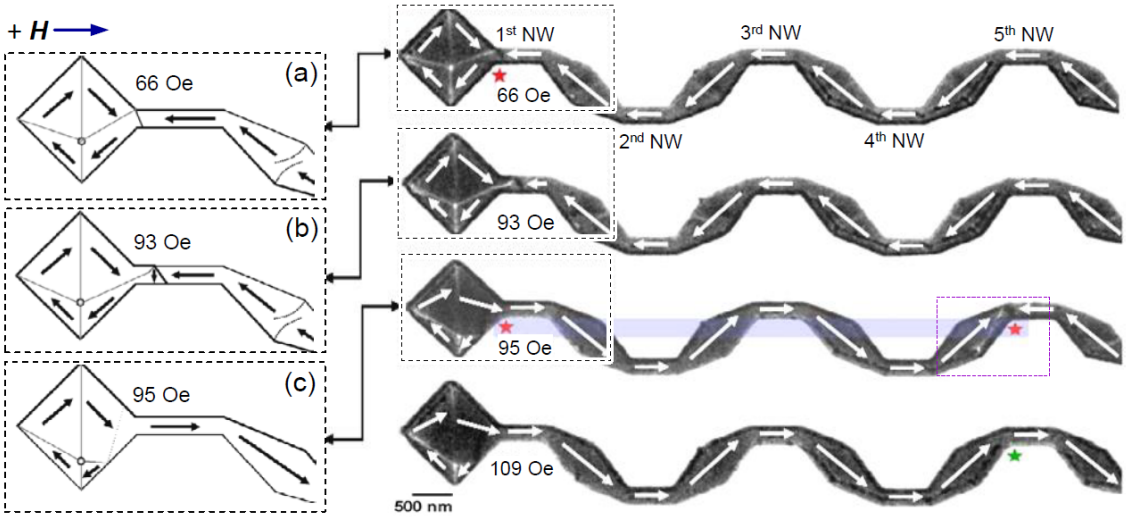

Fig. 8. Fresnel images of the DWT with a square injection pad recorded in the DW creation and propagation sequences. Therein, an external horizontal field was incrementally applied in the left-to-right direction aiming at creating a H2H-DW between the square pad and the left-end of the 1st-NW, as shown in Fig. 4(b). (a) A H2H DW created at 66 Oe, denoted as a red star. (b, c) Further increasing the propagation field strength, the created H2H DW slightly propagated along the 1st-NW at which the created DW distorted at the field strength of 93 Oe, it was then moved to the left end of the 5th-NW at the field strength of 95 Oe without stopping at any intermediate areas, indicated by pink stars. The wall annihilated out the structure at 109 Oe, indicated as a green star. (Reproduced from Ref. [18]).

applies to the DWT, the ability to create a single DW in the first NW and move it in the remaining part of the DWT was not improved.

Similar to the previous process, the horizontal pulsed field applies to the DWT in the left-to-right direction, results are seen in Fig. 9(a). However, a new spin configuration in the square pad was created where it was started with the CCW chirality, as shown in Fig. 9(b), in contrast with the case of the CW one showed in Fig. 9(a). The square injection pad is virtually divided by four quasi-equal areas with the dark fringes, contrast with the bright ones in Fig. 9(a). The magnetic state of the DWT did not change even if H_{pulsed} = 117.5 Oe was applied (Fig. 9b$_{\text{I}}$). A H2H-DW was created, propagated through four NWs and finally stopped at the fourth diamond pad under H_{pulsed} = 118.6 Oe, Fig. 9b$_{\text{II}}$. This stopped DW is defined as the H2H CW-VDW, indicated by two white arrows. The pulsed field strength is contiuously increased, H_{pulsed} = 129.1 Oe, a T2T CCW-VDW additionally created in the fifth diamond pad, Fig. 9b$_{\text{III}}$. This could be explained as a large pulsed field was applied during a short period of 5 μs. This results in the creation of the H2H CW-VDW. Moreover, the spins located in the remaining part of the DWT are also affected at which the response times of those spins are however different and slower than the short pulsed duration of 5 μs. Resulting in the magnetic moments of the given part are delayed with a certain period, leading to create the said T2T CCW-DW. The created DWs are opposite in their chirality, the magnetic state of the entire DWT structure is subsequently easier to balance/reach the stable/metastable state. Therein, the energies of these two DWs are compensated to push the

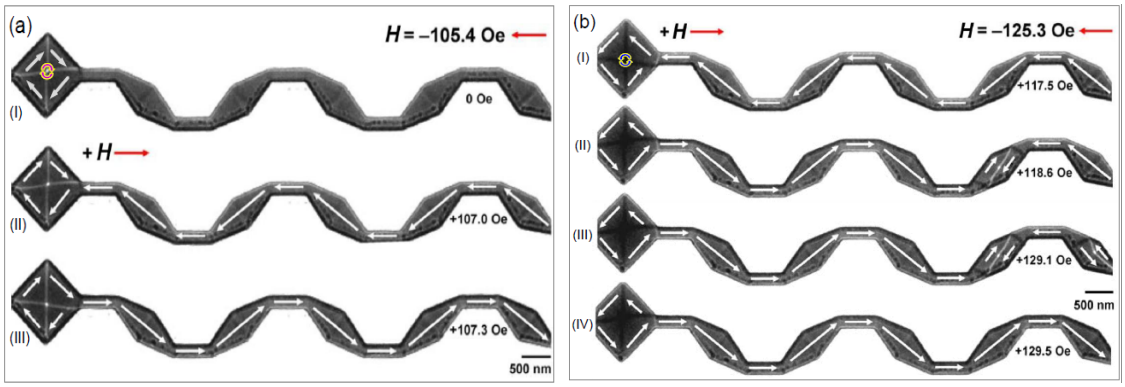

Fig. 9. (a) Fresnel images of the DWT with a square injection pad showing magnetization states in each NW at the saturation field of -105.4 Oe (a_I); the pulsed fields required to create/propagate/ remove a DW from the DWT ($a_{II,III}$). (b) Other Fresnel images of the said DWT recorded at the saturation field of -125.3 Oe at which the chirality of spins in the square injection pad was changed from the CW (a_I) to CCW (b_I) configuration. A H2H CW-VDW was created and propagated to the fourth diamond pad at the pulsed field of 118.6 Oe (b_{II}). Another T2T CCW-VDW was additionally created in the 5th pad at 129.1 Oe (b_{III}). Those walls removed out the DWT at 129.5 Oe (b_{IV}).

entire system to a lower energy level, as compared to the system consists of one DW. Those H2H CW- and T2H CCW-VDWs thus coexist. The pulsed field was continuously increased to H_{pulsed} = 129.5 Oe, those DWs were completely annihilated from the structure, leaving a quasi-saturated state of the given DWT, as seen in Fig. 9b_{IV}. As discussed, the use of pulsed fields did not increase the ability to create and propagate a single DW in such DWTs, adding extra DWs to the DWT makes the propagation characteristics of those DWs more complicated. If those DWs have different configurations, their movement directions are in opposite, leading to collision to create a new DW or destroy themselves. The results obtained from the same DWT with the use of the two given propagation methods showing that the role of various factors affecting the creation and propagation processes of DWs through the DWT: (*a*) the orientation of spins in the square pad; (*b*) the anisotropic factors of the DWT, i.e. a correlation of the square, NW and diamond sizes, the angle between the NWs and their connecting pads; (*c*) the effects of delayed times when applying a pulsed field on local magnetic moments in the diamond pads of the DWT.

V. CONCLUSION

The curved Py ($Ni_{80}Fe_{20}$) DWT nanostructures consist of five NWs were designed and studied. The magnetic properties of the created walls in those DWTs were investigated systematically using the Glasgow LTEM with both continuous and pulsed fields. The results of this work added some new findings for the nanomagnetism and nanotechnology research directions where controlling the creation and propagation of DWs in such curved 2D nanostructures is necessary. This is one of the important approaches to understand the principle of creating/controlling the movement of 'bit' information in future 3D recording/ reading devices and/or magnetic logic circuits. The results show that the shape properties of 2D NWs, the interconnection parts of those NWs and other related parameters directly affect the creation/propagation of those created DWs in the DWTs.

The transition process among wall types, STDW $\leftrightarrow$ ATDW $\leftrightarrow$ CW-VDW $\leftrightarrow$ CCW-VDW, and/or creating new DWs in such nanostructures, leading to the reproducibility of creating/propagating DWs is low/complex. Such instable behaviour could be explained as an effect from a combination factor of discrete parameters, i.e. connecting components, surface/edge roughness, chiral spins/orientations in/out-side the square injection pad. This leads us expand the research direction to study the influence of local defects onto the asymmetry of TDWs in which driving a DW to a specific location in such DWTs still needs to optimize in another study.

ACKNOWLEDGMENTS

The authors thank to Dr. Damien McGrouther, Dr. Sam McFadzean, Dr. Kerry J O'Shea, Prof. Stephen McVitie, Dr. Donald A. MacLaren and Prof. John N Chapman for experiment assistance and fruitful discussions. This work was supported by the Scottish Universities Physics Alliance (SUPA) Prize and Vietnam National Foundation for Science and Technology Development (NAFOSTED) under the project number: 103.02-2019.15.

REFERENCES

[1] S. S. P. Parkin, M. Hayashi and L. Thomas, *Science* **320** (2008) 190.
[2] D. A. Allwood, G. Xiong, M. D. Cooke, C. C. Faulkner, D. Atkinson, N. Vernier, R. P. Cowburn, *Science* **296** (2002) 2003.
[3] Y. Nakatani, A. Thiaville and J. Miltat, *Journal of Magnetism and Magnetic Materials* **290–291** (2005) 750.
[4] M. Kläui, *Journal of Physics: Condensed Matter* **20** (2008) R313001.
[5] L. Caretta, M. Mann, F. Büttner, K. Ueda, B. Pfau, C. M. Günther, P. Hessing, A. Churikova, C. Klose, M. Schneider, D. Engel, C. Marcus, D. Bono, K. Bagschik, S. Eisebitt and G.S.D. Beach, *Nature Nanotechnology* **13** (2018) 1154.
[6] M. A. Bahri, B. Borie, T. L. Jin, R. Sbiaa, M. Kläui and S. N. Piramanayagam, *Physical Review Applied* **11** (2019) 024023.
[7] X. Zheng, J. Wang, G. Li, X. Lu, W. Li, Y. Wang, Y. Chen, H. Yin, J. Wu and Y. Xu, *ACS Applied Electronic Materials* **2** (2020) 2375.
[8] T. J. Broomhall, A. W. Rushforth, M. C. Rosamond, E. H. Linfield and T. J. Hayward, *Physical Review Applied* **13** (2020) 024039.
[9] C. Brownlie, S. McVitie, J. N. Chapman and C. D. W. Wilkinson, *Journal of Applied Physics* **100** (2006) 033902.
[10] R. D. McMichael and M. J. Donahue, *IEEE Transactions on Magnetics* **33** (1997) 4167.
[11] D. Q. Hoang, M. T. Tran, X. H. Cao and D. T. Ngo, *RSC Advances* **7** (2017) 49188.
[12] V.N. M. Ho, L.D.A. Ho, M.T. Tran, X.H. Cao, V.A. Dao, D.H. Tong, D.T. Ngo and D.Q. Hoang, *RSC Advances* **8** (2018) 41828.
[13] K. J. O'Shea, *Putting a leash on the domain wall: a TEM investigation into the controlled behavior of domain walls in ferromagnetic nanostructures*, PhD thesis, University of Glasgow (2010) 37–38.
[14] M. A. Basith, S. McVitie, D. McGrouther, J. N. Chapman and M. R. Weaver, *Journal of Applied Physics* **110** (2011) 083904.
[15] L. D. A. Ho, M. T. Tran, X. H. Cao, V. A. Dao, D. T. Ngo and D. Q. Hoang, *RSC Advances* **8** (2018) 14539.
[16] `https://www.tedpella.com/` (cited 08/12/2020)
[17] J. N. Chapman, *Journal Physics D: Applied Physics* **17** (1984) 623.
[18] D. Q. Hoang, X. H. Cao, H. T. Nguyen and V. A. Dao, *Nanotechnology* **32** (2021) 095703.